POAC'13
Espoo, Finland

Proceedings of the 22nd International Conference on
Port and Ocean Engineering under Arctic Conditions
June 9-13, 2013
Espoo, Finland

MULTI-LEG STRUCTURES IN ICE – EXAMINING GLOBAL LOADING UNCERTAINTIES

A. Barker[1] and M. Sayed[1]

[1]National Research Council of Canada, Ottawa, CANADA

ABSTRACT

The ISO 19906 Arctic Offshore Standard (2010) represents a great advancement for standards as they pertain to Arctic engineering. However, uncertainties remain for a number of topic areas, including global loading on multi-leg structures in ice. These uncertainties include the effects of sheltering, the width of damaged ice and the effect of jamming. Additional uncertainties pertain to the effects of ridge loading and various ice properties. This paper numerically examines some of these uncertainties, through a parametric study approach. The results present the ice forces on a representative structure, as well as broken ice zone widths. The results show that peak loads are associated with ice drift at an angle, as observed in other laboratory and numerical simulations. In addition, loads increase with decreasing clearance between the legs. The results have applications not only for multi-leg oil and gas structures in ice-covered water, but could be further examined in the context of bridge piers and offshore fields of wind turbine towers.

INTRODUCTION

Barriers to development of oil and gas in the Canadian Arctic are largely due to environmental impacts and safety concerns related to failure of a structure from ice loading. With the publication of the ISO 19906 Arctic Offshore Structures Standard (2010), and its adoption by countries such as Canada, these new guidelines offer a concrete means of closing both the technological and knowledge barriers to such development. However, there are critical knowledge gaps that still exist, in the context of this paper, that relate to multi-leg platforms. For example, there is little guidance on ridge keel action, jamming, load dependence on ice movement direction, non-simultaneous action, maximum loads on different legs, loads at freeze-in conditions, or torsion moments. Yet each of these is critical for understanding of loads on a multi-leg platform.

Numerical studies of these parameters provide a relatively efficient way of investigating a variety of concerns. Results can be compared with what full-scale data may exist from instrumented offshore platforms (such as those located in Bohai Bay, China or Cook Inlet, Alaska), and factors that have not either been encountered in full-scale or have not been sufficiently documented can also be investigated.

For this study, a select set of conditions were chosen for investigation. They include:

- The effect of leg spacing on the ice forces;
- The effect of ice drift direction on the ice forces and any sheltering effects on the downdrift legs of a structure;
- Velocity effects on the ice forces;

- Ice thickness effects on the ice forces.

These topic areas have been identified by a number of ice experts as some of the more pressing concerns regarding the effectiveness of multi-leg structures in ice-covered waters. The present work deals with the case of a rigid structure. The effects of compliance of the structure are outside the scope of this paper.

NUMERICAL MODEL DESCRIPTION

The numerical formulation of the present model was described in a number of papers (e.g. Barker et al., 2000, Sayed and Barker, 2011 and Barker and Sayed, 2012).

The present model uses a continuum rheology that follows an extended von Mises plastic yield criterion. The governing equations consist of the continuum equations for the balance of linear momentum and the plastic yield criterion. Those equations are solved using a fixed grid. The numerical solution is based on a hybrid Eulerian-Lagrangian approach, which is suited for handling large deformations, discontinuous behaviour and moving boundaries. The structure is modeled as a rigid-body. The approach is based on using an implicit finite difference solution of the momentum equations. A Particle-In-Cell (PIC) method is used to advect the ice. That method employs discrete particles to represent the ice and cover. Each particle is assigned several attributes that describe the state of the ice cover, such as velocities, ice concentration and thickness. Those particles are advected in a Lagrangian manner. At each time step of the solution, the momentum equations are solved to determine ice stresses and velocities, as well as the forces on the structure. The updated variables (e.g. velocities and accelerations) are then mapped to the particles, which are advected to new positions. From the new positions, the attributes of the particles are mapped back to the grid, and the solution steps are repeated.

Boundary conditions are introduced by specifying the values of the acceleration and velocity to represent a no-slip or a full-slip condition. Friction forces can also be specified at those boundaries. The stress-free surface does not require special treatment. For the present study, a Coulomb friction boundary condition is applied at the interface between the ice and the structure; i.e. the tangential stress is proportional to the normal stress and acts along a direction opposite to that of ice velocity. At the upstream boundary of the ice cover, a constant velocity is used as a boundary condition.

For the present case, the horizontal distances are much larger than ice thickness. Therefore, a depth-averaged approach is used in the simulations. In this case, the stresses and velocities are considered to be uniform over the thickness of the ice. Thickness variations, however, are accounted for. As stresses exceed a threshold, representing a ridging stress, each particle undergoes ridging; i.e. the thickness increases and area decreases, while conserving ice volume. Future efforts in this study will examine the effects in three-dimensional scenarios, in order to investigate the influence of a variety of parameters on the pressure distribution on the structure's legs, for example.

PARAMETRIC STUDY

The parameters of the present test cases are shown in Table 1. The ice concentration remained the same throughout the test series (0.95), as did the friction coefficient (0.2) and ice strength. Similarly, the leg diameters remained constant, at 6 m. The structure is considered to be rigid and is introduced using a no-slip boundary condition. The initial leg spacing, from the centreline of one leg to the centreline of another, was 28 m. The basic grid layout is

shown in Figure 1. The initial ice thickness was chosen as 2 m. While this represents a very thick first year ice cover, it was chosen to represent relatively high load cases that are relevant to design conditions for regions such as the Beaufort Sea. A thinner ice sheet was subsequently simulated in the parametric study, which is similar to average conditions for regions such as the Cook Inlet (see, for example, Matskevitch et al, 2007).

For the base case, the ice drift direction is at 90° to the structure. The structure was then rotated to simulate two other drift directions, 30° and 45° (Figure 2). In addition, the leg spacing was decreased in all directions, from the base case condition down to 24 m and then 20 m. All three distances represent an L/W value of less than 4 (where L is the clear distance between legs and W is the leg diameter). As indicated in the ISO 19906 Arctic Offshore Structures Standard (2010), an L/W value of less than 4 is more likely to induce jamming between the structure's legs.

Table 1. Parametric study scenarios.

Test #	Description of test, as variation from Base Case	Centreline Leg Spacing (m)	Angle of Ice Approach (°)	Ice Velocity (m/s)	Ice Thickness (m)
M1	Base Case	28	90	0.5	2
M2	Drift direction 45°	28	45	0.5	2
M3	Drift direction 30°	28	30	0.5	2
M4	Slower velocity, Drift direction 90°	28	90	0.2	2
M5	Slower velocity, Drift direction 45°	28	45	0.2	2
M6	Slower velocity, Drift direction 30°	28	30	0.2	2
M7	More narrow, Drift direction 90°	24	90	0.5	2
M8	More narrow, Drift direction 45°	24	45	0.5	2
M9	More narrow, Drift direction 30°	24	30	0.5	2
M10	More narrow, Drift direction 90°	20	90	0.5	2
M11	More narrow, Drift direction 45°	20	45	0.5	2
M12	More narrow, Drift direction 30°	20	30	0.5	2
M13	Thinner ice, Drift direction 90°	28	90	0.5	0.75
M14	Thinner ice, Drift direction 45°	28	45	0.5	0.75
M15	Thinner ice, Drift direction 30°	28	30	0.5	0.75

SIMULATION RESULTS

Table 2 summarizes the forces that were recorded on each leg, as well as the global force on the structure and widths of damaged ice. Note that the maximum forces recorded were not necessarily simultaneous. In the simulations, the only occasions where the maximum loads were indeed simultaneous were during the initial contact of the ice sheet with two legs at the same time (for example, in the 90° or 45° simulations, on some occasions). The structure is not represented as a compliant structure, so this intuitively makes sense. The width of damaged ice was taken as the perpendicular distance from one leg of the structure to the area where the ice was deformed to 40% of the original ice thickness, either to the along-drift side of the structure, or updrift.

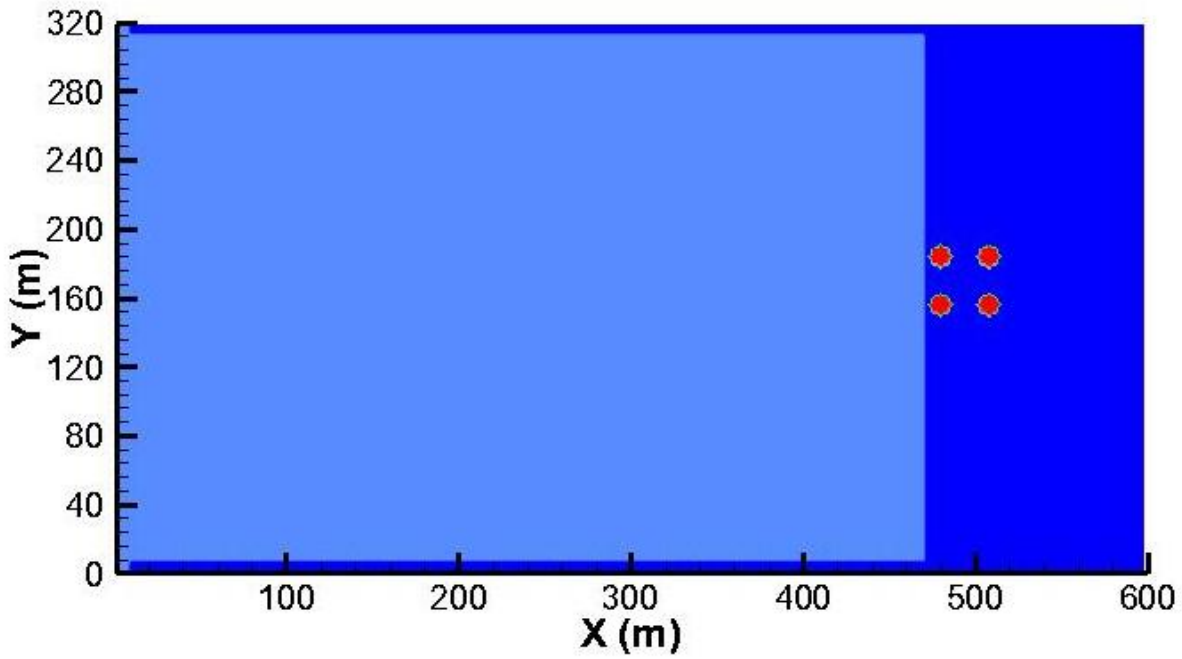

Figure 1. Image of the Base Case grid layout. The ice sheet, shown in pale blue, moves from left to right, impacting the structure, shown in red.

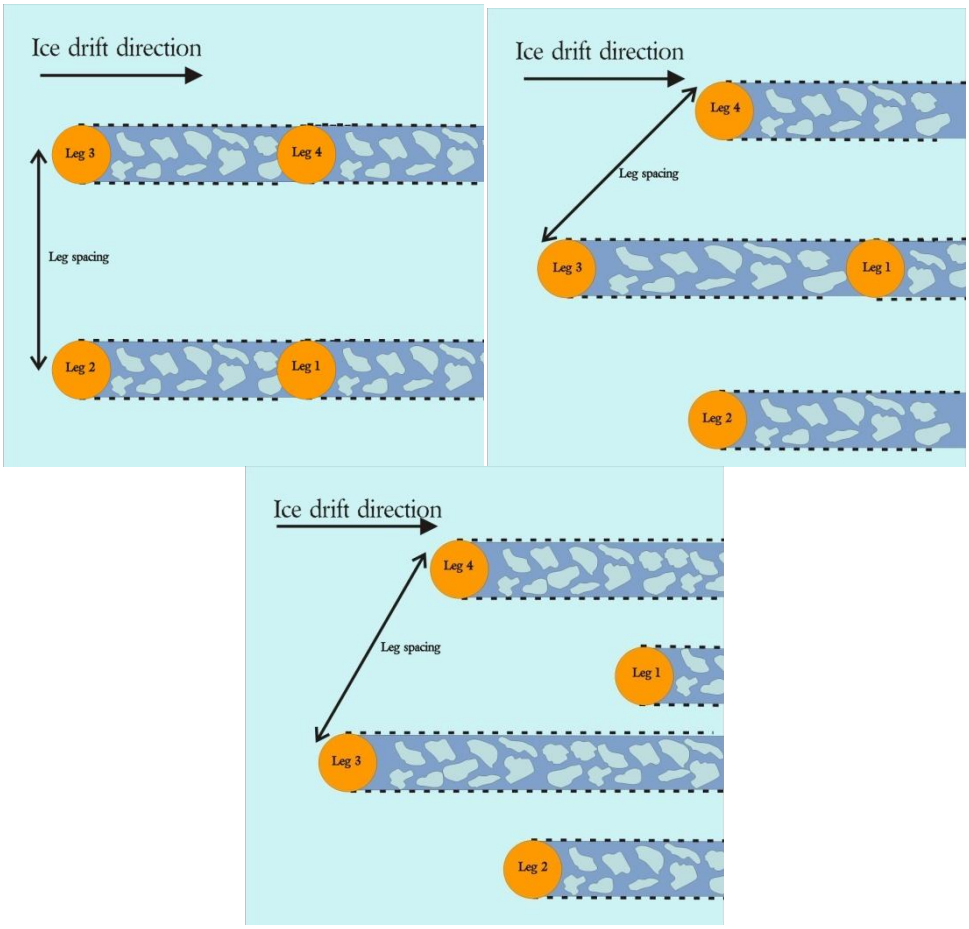

Figure 2. The three configurations that were examined: ice drift direction at 90° to the structure, 45° and 30°.

Table 2. Parametric study results. Maximum measured and 98th percentile loads are presented.

Test Number		Global Load (MN)	Load Leg 1 (MN)	Load Leg 2 (MN)	Load Leg 3 (MN)	Load Leg 4 (MN)	Width of Damaged Ice – Updrift (m)	Width of Damaged Ice – Sides (m)
M1	Max	23	5	8	8	6	8	5
	98%	22	5	8	7	6		
M2	Max	32	8	8	8	10	14	7
	98%	31	7	8	7	10		
M3	Max	28	8	8	8	9	18	7
	98%	27	7	8	7	9		
M4	Max	17	5	7	7	5	20	5
	98%	17	5	7	7	4		
M5	Max	29	8	8	8	9	7	5
	98%	27	6	8	7	9		
M6	Max	27	9	7	8	8	8	5
	98%	26	8	7	7	8		
M7	Max	24	5	8	8	5	6	5
	98%	23	5	8	8	5		
M8	Max	32	3	9	11	16	15	10
	98%	32	2	9	10	15		
M9	Max	32	4	4	12	18	16	8
	98%	30	3	4	12	17		
M10	Max	27	6	8	13	9	10	7
	98%	26	5	7	12	8		
M11	Max	35	0	5	14	20	14	10
	98%	34	0	5	13	19		
M12	Max	31	4	3	12	22	15	10
	98%	31	3	3	12	21		
M13	Max	14	4	4	3	5	2	4
	98%	14	4	4	3	5		
M14	Max	15	3	4	3	5	11	5
	98%	15	3	4	3	5		
M15	Max	15	4	4	3	5	13	7
	98%	15	4	4	3	4		

Leg 3, which was the leading leg when the ice drift was at 30° or 45°, generally experienced the highest load upon initial impact of the ice. Subsequent loading on that leg could approach, or sometimes equal, the initial impact, but it never exceeded the initial impact load. As an example, Figure 3 shows the force-time output for case M11, which corresponds to a direction angle of 45^{o}. The highest force was on Leg 4, which is not the front leg. Leg 3, at the front experienced a lower force. This finding appears counter-intuitive. Possible causes for that behaviour may be that the failure mode of the ice cover against the front leg was primarily splitting as evidenced by large cracks (or leads) that appear in the thickness and concentration contours. The back leg was impacted by the thicker ice that sheds upon encountering the front leg and may have failed mostly in compression (crushing). We note here that once ice breaks into rubble, its strength is reduced in the simulations (e.g. tensile strength drops to zero). This cursory explanation is somewhat speculative. More systematic examination of this issue needs to be done.

Force records also showed that larger increases in the global load on the whole structure were often associated with large loads on Leg 1, which is the trailing leg when the ice drift was at 30° or 45°.

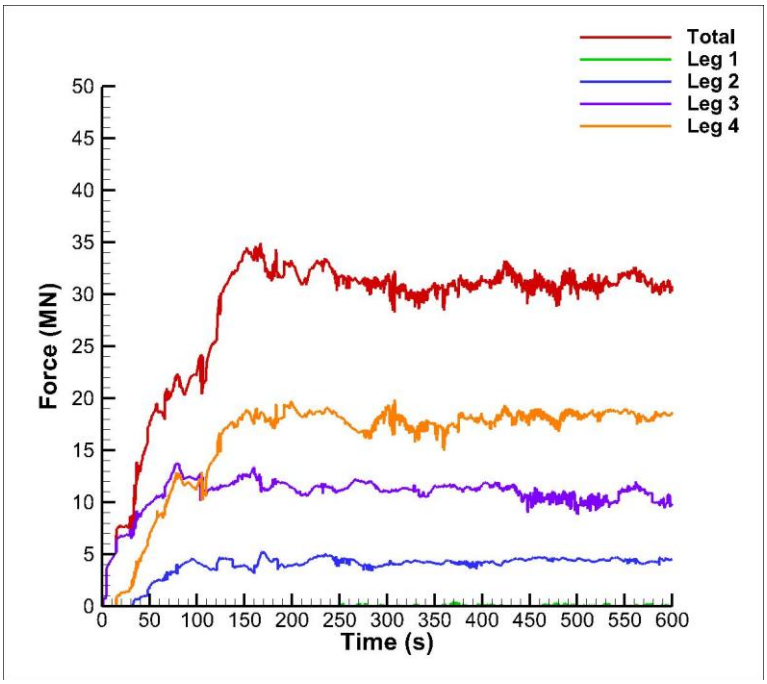

Figure 3. Force output for simulation M11, with a leg spacing of 20 m and with an ice drift angle of 45°. This was one of the highest force records for the series. The is little to no loading on Leg 1.

Figure 4 is an image of the product of the ice thickness multiplied by the ice concentration. Plotting the results of the simulations in this manner provides a more clear indication of regions of thicker, highly concentrated ice compared to areas of thin, low concentration or undeformed ice. For the base case (Figure 4a), it can be seen that while complete jamming did not occur, there was a pile-up of ice building up between the two downdrift legs of the structure. In comparison, for simulation M4 (Figure 4b), which was the same as the base case except with a slower ice drift velocity, the build up was occurring at the updrift side of the structure. While the width of the deformed ice for both cases was similar at the sides of the structures (5 m), simulation M4 had a greater pile-up of deformed ice at the updrift side of the structure (20 m versus 8 m for the base case).

The focus of the present study was on force distribution on the legs of the structure. Conditions leading to jamming between the legs were not explored in detail. Jamming, however, was observed in a few cases. Case M6 showed evident jamming. This is expected because of the 30^{o} angle, and the relatively lower ice velocity. Figure 5b shows the shape of that jam formation. We also note that another factor that is likely to affect jamming is floe size distribution. That factor should be considered in any treatment of jamming conditions. The present simulations, however, deal with intact ice covers. That corresponds to ice covers consisting of very large floes (compared to the size of the structure).

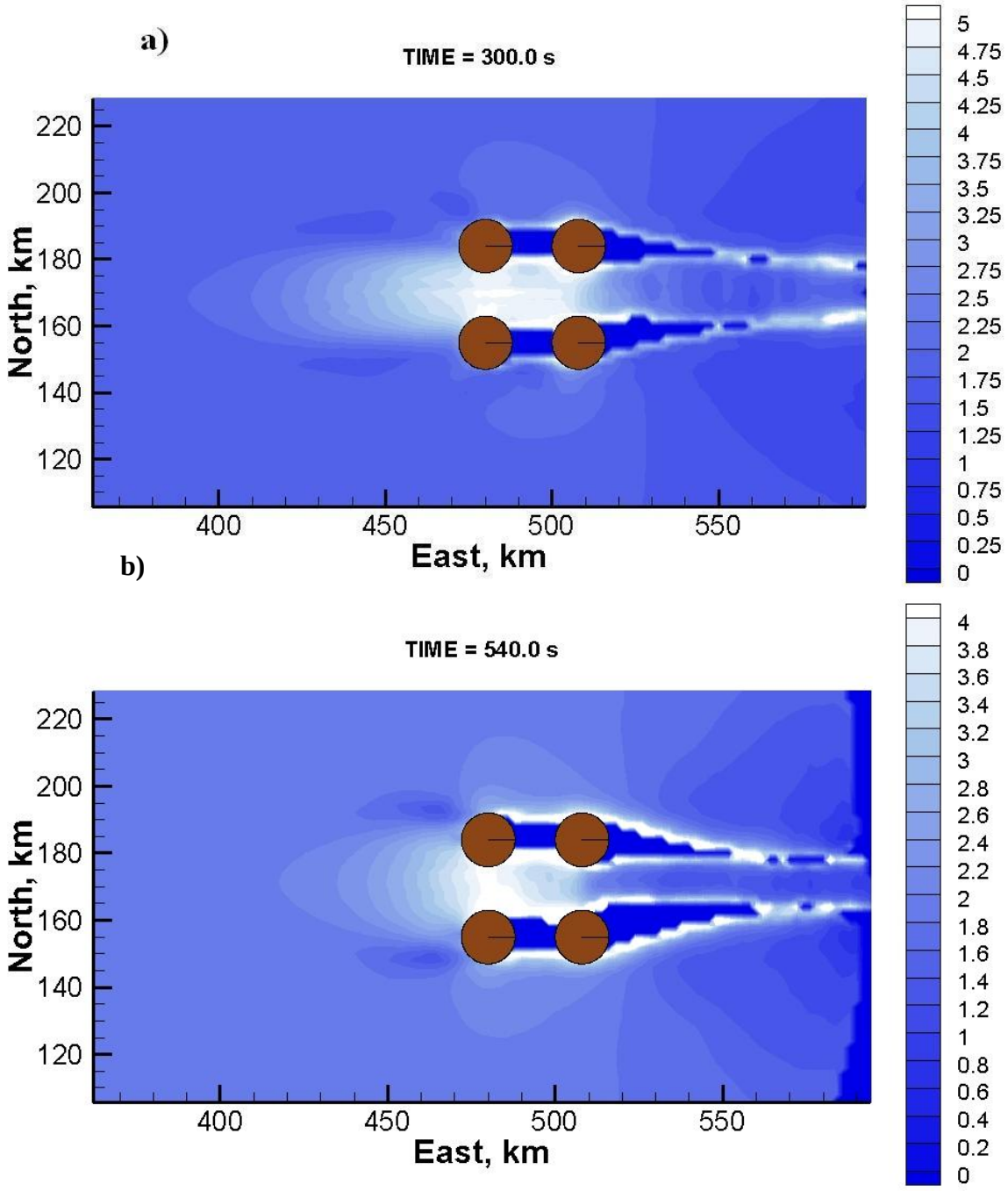

Figure 4. Plots of the product of ice thickness multiplied by ice concentration for a) the base case. The image demonstrates areas of thick, highly concentrated ice, as shown in the bright white bands of colour, as well as thin, low concentrations of ice, shown in the paler white and blue coloured areas. The width of the highly damaged zone of ice is relatively tight to the structure, extending approximately 5 m away from the legs on the sides of the structure and 8 m on the updrift side of the structure; b) simulation M4, one of the slower velocity simulations.

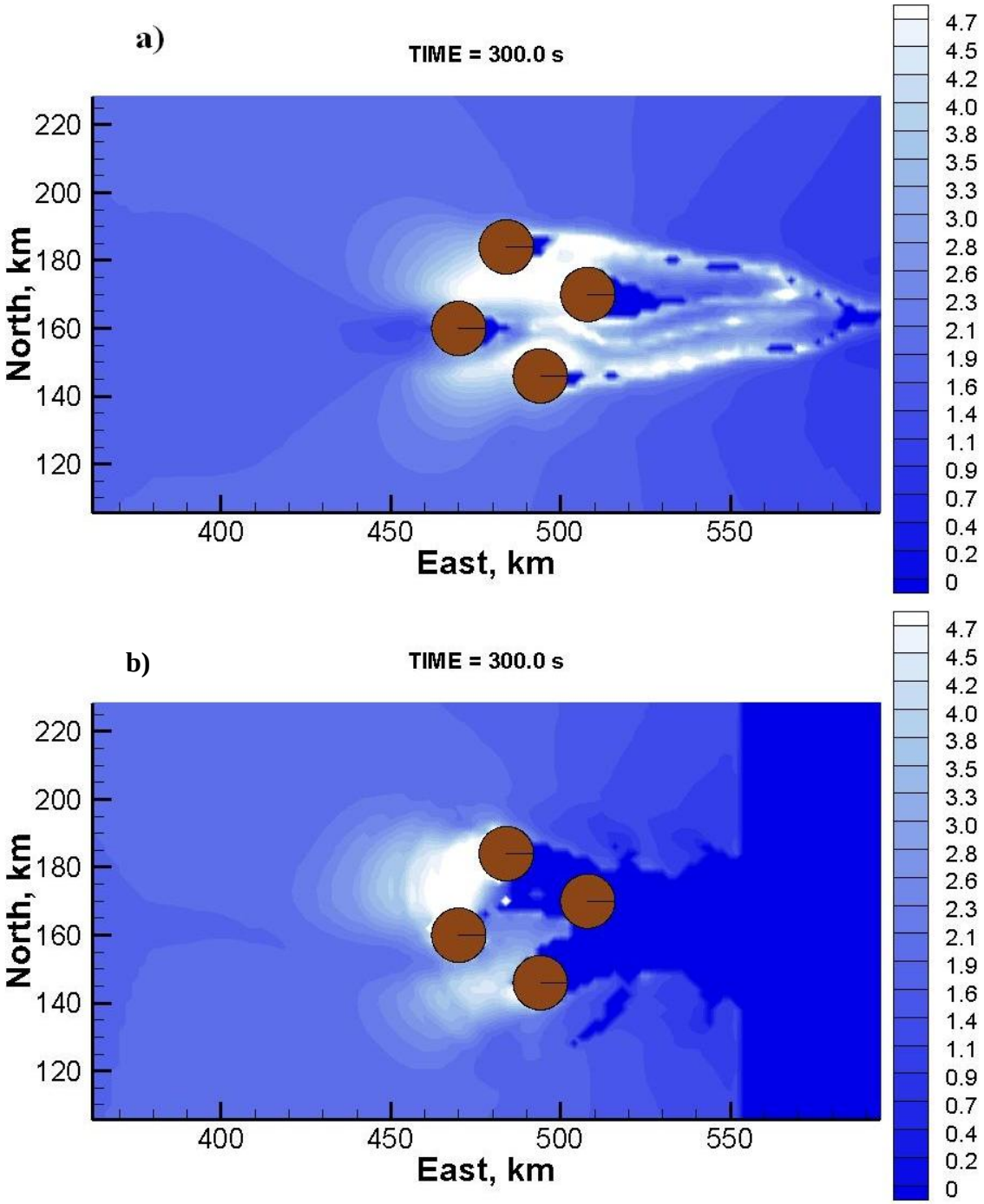

Figure 5. Plots of the product of ice thickness multiplied by ice concentration for a) simulation M3, with a 30° ice drift direction and b) simulation M6, with a 30° ice drift direction and velocity of 0.2 m/s. It can be seen how the patterns of ice deformation vary from the base case at both the updrift and downdrift sides of the structure, and between the four legs. The slower ice movement apparently produced jamming.

Takeuchi et al (1993) reported on a study of multi-leg structures. They found that the peak loads on a four-legged structure occur with ice drift direction angle in the range of 26° to 27°. In the present study, Figure 6 indicates that the forces were a slightly higher for the 45° angle simulations, and increased as well for those simulations with a higher velocity. The effect of leg spacing is illustrated in Figure 7, which indicates that force on the structure increased for smaller values of the spacing between the legs. The smaller values of spacing may correspond

to some degree of *arching*, even if without jamming. That arching would increase stresses in the ice cover and the forces. For the 30° angle in Figure 7, the smallest two values of spacing between the legs produced nearly identical forces.

In Figure 8, the relationship between the global load and the width of damaged ice may be seen. There was a general trend of increasing global load with increasing damage width. Of interest, the damage zone in front of the structure at 30° ice drift direction was more highly damaged in front of two of the lagging legs, rather than Leg 3, which the ice first impacted. This is shown in Figure 5.

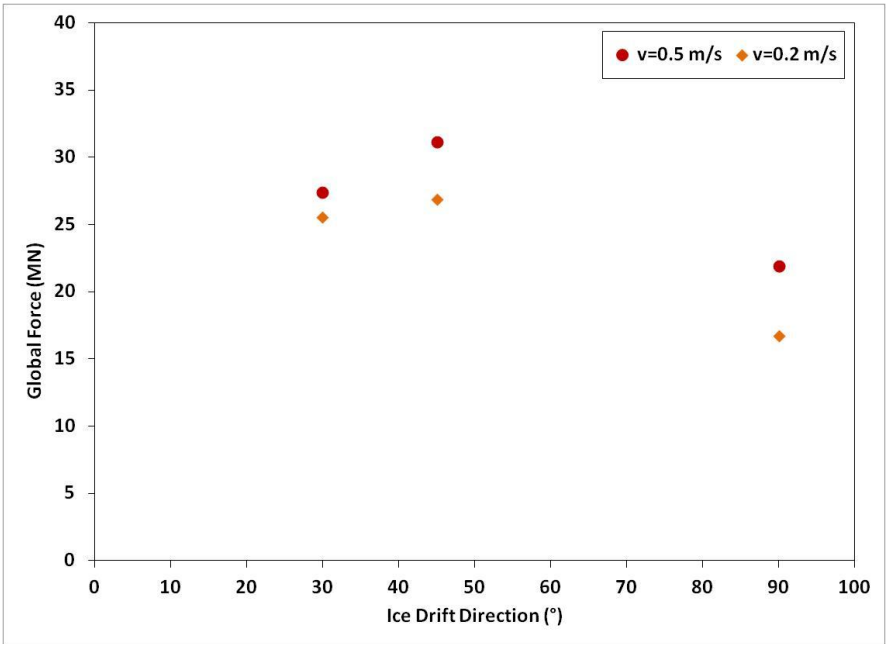

Figure 6. Plot of global force (98%) as a function of ice drift direction and velocity. The higher velocity simulations consistently had higher forces compared to the slower velocities.

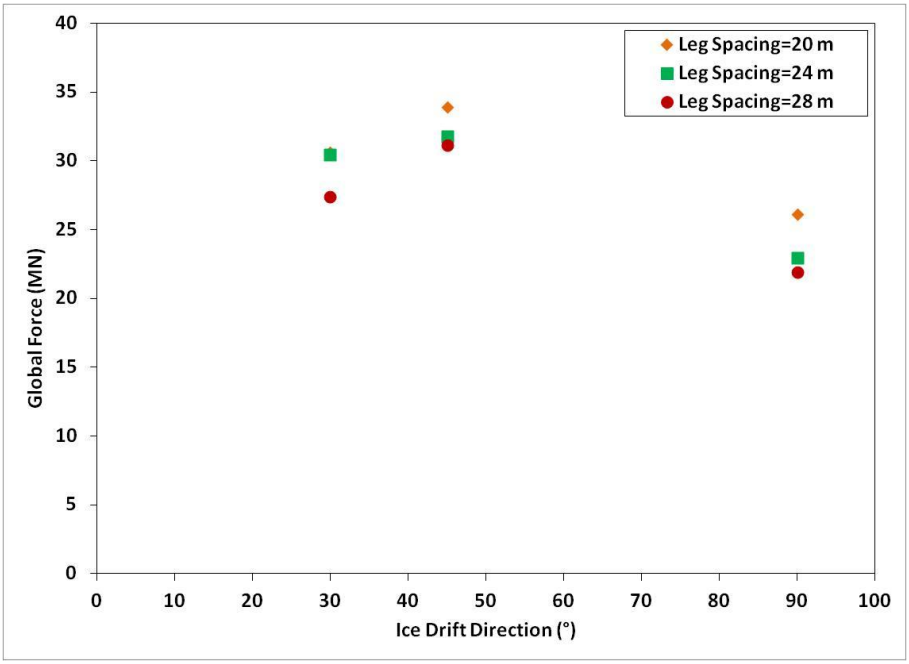

Figure 7. Plot of global force (98%) as a function of ice drift direction and leg spacing.

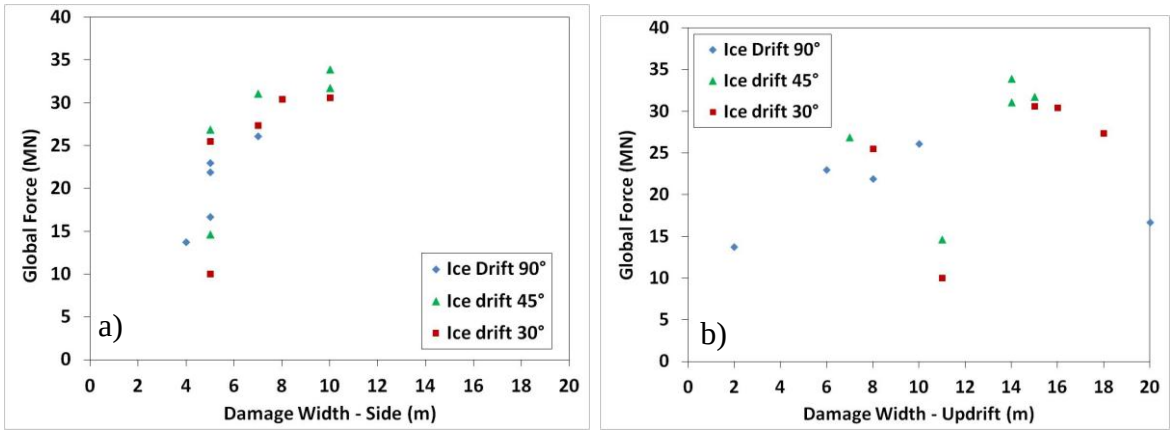

Figure 8. Plot of the global load (98%) and the width of damaged ice for a) the side of the structure and b) updrift of the structure.

COMPARISON WITH THE ISO 19906 STANDARD AND OTHER ICE LOAD ESTIMATES

Results of the simulations can be compared with analytical methods, other simulations and measured full-scale loads. The ISO 19906 Arctic Offshore Structures Standard (2010) provides guidance on the determination of the global loading on a multi-leg structure. The method presented for determination of the global load on a single leg, F_G (in MN), is:

$$F_G = p_G * h * w \quad [1]$$

where p_G is the global pressure (MN), h is ice thickness (m) and w is structure width (m). The global pressure can be calculated as:

$$p_G = C_R \, (h/h1)^n (w/h)^m \quad [2]$$

where w is the projected width of the structure (m), h thickness of the ice sheet (m), $h1$ a reference thickness of 1 m, m an empirical coefficient that depends upon the aspect ratio (w/h) and is equal to −0.16; n an empirical coefficient on ice thickness equal to −0.50 + h/5 for h < 1.0 m, and to −0.30 for h ≥ 1.0 m and C_R ice strength coefficient (MPa), here taken to be 2.3, representing a value mid-way between the recommended values for Baltic and Beaufort ice (ISO, 2010). To determine the global load on the structure, rather than one leg, guidance is provided as:

$$F_S = k_s \, k_n \, k_j \, F_1 \quad [3]$$

where F_1 is the ice action on one leg (F_G, as calculated above), k_s accounts for the interference and sheltering effects (with values between 3 and 3.5 for maximal sheltering), k_n accounts for the effect of non-simultaneous failure (is equal to 0.9, where no data exists), and k_j accounts for the ice jamming (no guidance provided for a value). These formulas give a load on an individual leg of 19 MN, and a global load on the structure of 60 MN. These results are approximately double those of the simulated loads. Using a C_R value of 2.8, for Beaufort-type conditions, gives a global load of 72 MN (individual leg load of 23 MN).

Määttänen and Kärnä (2010) suggested that the ISO 19906 (2010) approach is non-conservative for *w/h* values of less than 10, which would apply to the present scenarios. In addition, Frederking (2012) compared a variety of standards' methods for determining the

global load on a multi-leg structure. He determined that for an example scenario with a structure that had 18 m diameter legs and an ice thickness of 1.2 m, the various codes gave global pressures that converged to a range of pressure between 1.25 and 2 MPa. This results in single leg loads of approximately 26 to 38 MN and global loads between approximately 90 and 150 MN. These calculated loads are considerably larger than the loads obtained from the simulations.

A study by Vachon et al. (2012), which also used the present numerical model, obtained similar results to this study, with global forces of approximately 20 MN for 2m thick ice impacting a multi-leg structure that had individual leg diameters of 10 m, spaced 80 m apart. With decreasing velocity, the loads given by Vachon et al. (2012) also decreased, as they did with decreasing ice thickness. Unlike the present study, the loads decreased with changing ice drift direction, resulting in lower loads for an ice drift at 45°. The leg spacing of the Vachon et al. (2012) study was much larger than the present one, however, so this may have caused that discrepancy. Vachon et al. (2012) examined loads on an existing jam. With those simulations, the loads on the structure were considerably greater, in the order of 90 MN, almost a 5-fold increase over the conditions without an ice jam and similar to the associated 5-fold increase in contact width. In Karulin et al. (2012), laboratory and numerical simulations for a semisubmersible floating drill rig were conducted. While the nature of the structure is different, similarly ice drift at 45° produced the highest loads.

Concerning field measurements, Kärnä and Yan (2006) provided an extensive analysis of full scale measurements on the Norströmsgrund lighthouse. They calculated pressures associated with the maximum loads of approximately 0.4 MPa, for ice thicknesses greater than 1 m. This is lower than the values calculated with ISO 19906 (2010), and more in line with some of the present simulation results. Using the value of 0.4 MPa, for the present structure, a load of approximately 5 MN is obtained. Other information on multi-leg structures was reported by Matskevitch et al. (2007). They discussed design ice loads for a number of platforms in Cook Inlet, Alaska, which varied between 21 and 63 MN. The higher loads are associated with a design ice pressure (2.1 MPa) acting on all four legs simultaneously. Maximum full-scale loads inferred from some of the Cook Inlet platforms, also presented in Matskevitch et al. (2007) ranged from 5 to 7 MN. Those latter estimates are lower than the design values; thickness values were not indicated. Additional field data comes from the platforms in the Bohai Sea. Johnston et al. (2000) examined a load trace from the JZ-20 platform, which has smaller dimensions then the present tests. For that platform, the loads were considerably smaller than the present simulation, with measured global loads around 150 kN on two of the legs for level ice thicknesses in the order of 0.25 m and rafted of 0.6 m.

SUMMARY

The present paper examined aspects of ice interaction with multi-leg structures. The work was motivated by the need to clarify several critical issues not included in the guidance provided by the recent ISO 19906 standard. In particular, the effects of sheltering of back legs, direction of ice movement and the extent of damaged ice were examined. The approach employed numerical simulations based on solving the conservation of mass and momentum together with a plastic yield condition. The simulations predict the evolution of the distributions of stresses deformation of the ice cover as well as the forces on each leg of the structure.

The ISO standard, as all design codes, is intended to give safe upper limit values of expected forces. The predicted forces are lower than the values given by the ISO 19906 standard. They

are somewhat close, however, to reported estimates from field measurements. The total forces and those on individual legs were determined for a range of ice movement directions. The effect of sheltering of trailing legs was quantified. The front legs usually experienced the highest forces, compared to the back legs. In some cases for simulations at 30° or 45°, however, Leg 4 experienced higher forces than the leading leg. A plausible explanation for that counter-intuitive result is that failure mode against the leading leg was predominantly splitting of the ice cover. In some instances a trailing leg would encounter the thicker ice (that cleared around the front leg) which fails in compression. Further work is need, though, to clarify this issue.

Future work will further examine the mechanics of sheltering and force reduction on the back legs of the structure. Planned work will also examine forces due to ridges, the role of ice-structure friction, and a detailed study of jamming. The effort will include more detailed comparisons with available measurements. Further, expanded results can be used for probabilistic analysis of scenarios that are relevant to multi-leg structures operating in ice-covered water. By closing the knowledge gaps that exist, this will lead to a stronger standard that both Regulators and Industry will have a greater confidence in applying.

ACKNOWLEDGEMENTS

The authors would like to acknowledge the financial support of the Program on Energy Research and Development's Offshore Environmental Factors programme. Thank you to R. Frederking for his comments and suggestions for this research project.

REFERENCES

Barker, A., Timco, G., Sayed, M., Wright, B. 2000. Numerical Simulation of the "Kulluk" in Pack Ice Conditions. Proceedings of the 15th IAHR International Symposium on Ice, Volume 1, pp 165-171, Gdansk, Poland.

Barker, A. and Sayed, M. 2012. Upward- or Downward-Breaking Cones in Ice: Which One Should You Use? Proceedings Cold Regions Engineering 2012: Sustainable Infrastructure Development in a Changing Cold Environment, pp 715-724. Quebec City, Canada.

Frederking, R. (2012) Comparison of Standards for Predicting Ice Forces on Arctic Offshore Structures. Proceedings of the Tenth (2012) ISOPE Pacific/Asia Offshore Mechanics Symposium, pp. 60-67. Vladivostok, Russia.

ISO 19906, 2010. Petroleum and natural gas industries-Arctic offshore structures. International Organization for Standardization. Geneva, Switzerland.

Johnston, M.E., Timco, G.W., Frederking, R., Jochmann, P. 2000. Simultaneity of Measured Ice Load on Two Legs of A Multi-Leg Platform. Proceedings OMAE'00, Paper 00-1007, New Orleans, USA.

Kärnä, T., and Yan, Q., "Analysis of the Size Effect in Ice Crushing edition 2". Internal Report RTE50-IR-6/2005, Technical Resreach Centre of Finland, VTT Building and Transport, 2006.

Karulin, E., Karulina, M., Toropov, E., and Yemelyanov, D. 2012. Influence of Ice Parameters on Managed Ice Interaction with Multi-legged Structure. Proceedings of the 21st IAHR International Symposium on Ice, pp907-919. Dalian, China.

Määttänen, M. and Kärnä, T., 2011. ISO 19906 Ice crushing load design extension for narrow Structures. Proceedings of the 21st International Conference on Port and Ocean Engineering under Arctic Conditions, paper POAC11-063. Montréal, Canada.

Matskevitch, D.G., Spring, W., Timco, G.W. and Barker, A. (2007) Ice-structure interaction studies on the Granite Point Platform. Proceedings of the 8th International Conference and Exhibition for Oil and Gas Resources Development of the Russian Arctic and CIS Continental Shelf, RAO/CIS Offshore'07, St. Petersburg, Russia.

Sayed, M., and Barker, A. 2011. Numerical simulation of ice interaction with a moored structure. Proceedings of the Arctic Technology Conference (ATC), paper OTC 22101. Houston, U.S.A.

Takeuchi, T., Saeki, H. and Yamashita, T. (1993) Total Ice Forces on Multi-Legged Offshore Structures. Proceedings of the Third International Offshore and Polar Engineering Conference, pp. 532 – 537. Singapore.

Vachon, G., Sayed, M. and Kubat, I. (2012) Determination of Ice Management Efficiency. Proceedings of the 10th International Conference and Exhibition of Performance of Ships and Structure in Ice (IceTech 2012). Paper Number ICETECH12-106-R0. Banff, Canada.